

Singlet ground state in the spin-1/2 dimer compound $\text{Sr}_3\text{Cr}_2\text{O}_8$

Yogesh Singh and D. C. Johnston

Ames Laboratory and Department of Physics and Astronomy, Iowa State University, Ames, IA 50011

(Dated: September 13, 2018)

Magnetic susceptibility χ and specific heat C versus temperature T measurements on polycrystalline samples of $\text{Sr}_3\text{Cr}_2\text{O}_8$ and the isostructural, nonmagnetic compound $\text{Sr}_3\text{V}_2\text{O}_8$ are reported. A Curie-Weiss fit to the high- T $\chi(T)$ data for $\text{Sr}_3\text{Cr}_2\text{O}_8$ indicates that the Cr atoms are in the rare Cr^{5+} (Spin $S = 1/2$) valence state as expected from the composition. The ground state was found to be a spin singlet with an excitation gap $\Delta/k_B = 61.9(1)$ K to the magnetic triplet states, and a weak interdimer coupling of 6(2) K was inferred. The C and χ measurements on $\text{Sr}_3\text{V}_2\text{O}_8$ reveal a phase transition at 110 K which is evidently a structural transition.

Systems with a spin singlet ground state have been extensively studied because of the various quantum phenomena like Bose-Einstein condensation (BEC) of magnons^{1,2,3,4} and the Wigner crystallization of magnons,⁵ that are observed when the spin gap is closed continuously with the application of a magnetic field. The phenomenon of magnon-BEC which was first experimentally observed in TlCuCl_3 [1] has since been observed in other materials like the quasi-one dimensional (1D) material $\text{Pb}_2\text{V}_3\text{O}_9$,² and the quasi-2D materials $\text{BaCuSi}_2\text{O}_6$ [3] and Cs_2CuCl_4 .⁴ On the other hand, the Wigner crystallization of magnons was reported to be realized in the orthogonal dimer system $\text{SrCu}_2(\text{BO}_3)_2$ with the Shastry-Sutherland lattice.⁵ These discoveries have accelerated the search for new spin dimer systems and new quantum phenomena.

Recently the compounds $\text{Ba}_3\text{Mn}_2\text{O}_8$ [6,7,8] and $\text{Ba}_3\text{Cr}_2\text{O}_8$ [9] have been reported to be new spin-1 and spin-1/2 dimer compounds, respectively. $\text{Ba}_3\text{Mn}_2\text{O}_8$ exhibits a magnetization plateau at half of its saturation magnetization^{6,8} like in $\text{SrCu}_2(\text{BO}_3)_2$.⁵ The compound $\text{Sr}_3\text{Cr}_2\text{O}_8$, isostructural with $\text{Ba}_3\text{Cr}_2\text{O}_8$, was first found in a study of the SrO-Cr oxide phase diagram.¹⁰ The structure¹¹ is shown in Fig. 1. However, its magnetic properties have not been investigated. We have prepared polycrystalline samples of $\text{Sr}_3\text{Cr}_2\text{O}_8$ which contains Cr in the unusual 5+ valence state as expected from the composition, and of the isostructural, nonmagnetic compound $\text{Sr}_3\text{V}_2\text{O}_8$ for comparison. Herein we report the results of magnetic susceptibility χ and heat capacity C versus temperature T measurements on these samples. Analysis of the data indicates that $\text{Sr}_3\text{Cr}_2\text{O}_8$ is a new spin-1/2 dimer compound with antiferromagnetic exchange couplings, and with a zero-temperature spin gap $\Delta/k_B = 62$ K and a small inter-dimer coupling ≈ 6 K. $\text{Sr}_3\text{V}_2\text{O}_8$ undergoes a phase transition below 110 K which is evidently a structural transition.

Polycrystalline samples of $\text{Sr}_3\text{Cr}_2\text{O}_8$ and $\text{Sr}_3\text{V}_2\text{O}_8$ were prepared by solid state synthesis. The starting materials SrCO_3 (99.99%, Alpha Aesar) and Cr_2O_3 (99.99%, Alfa Aesar) or V_2O_5 (99.995%, MV Labs) were taken in stoichiometric proportion and mixed thoroughly in an agate mortar. The mixture was pressed into a 1/4-inch pellet, placed in a covered Al_2O_3 crucible and heated in air at 1200 °C for 24 hrs and then air quenched to room tem-

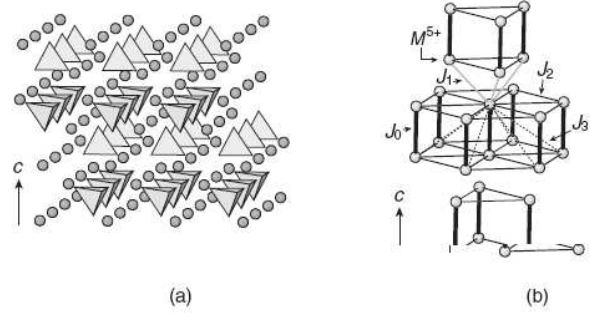


FIG. 1: (a) The crystal structure^{9,11} of $\text{Sr}_3\text{Cr}_2\text{O}_8$ constructed from CrO_4 tetrahedra and Sr ions (solid spheres). (b) The arrangement of Cr^{5+} ions (open spheres) in the $\text{Sr}_3\text{Cr}_2\text{O}_8$ crystal structure. The shortest Cr-Cr bond is represented by thick black lines. J_0 , J_1 , J_2 and J_3 denote the first, second, third and fourth nearest-neighbour interactions. From Ref.9

perature. After the initial heat treatment the material was reground and pressed into a pellet and given two similar heat treatments of 24 hrs each with an intermediate grinding after the first 24 hrs. Hard well-sintered pellets were obtained. Part of the pellet was crushed for powder x-ray diffraction (XRD). The XRD patterns were obtained at room temperature using a Rigaku Geigerflex diffractometer with $\text{Cu K}\alpha$ radiation, in the 2θ range from 10 to 90° with a 0.02° step size. Intensity data were accumulated for 5 s per step. The $\chi(T)$ was measured using a commercial Superconducting Quantum Interference Device (SQUID) magnetometer (MPMS5, Quantum Design) and the $C(T)$ was measured using a commercial Physical Property Measurement System (PPMS5, Quantum Design).

All the lines in the X-ray patterns of $\text{Sr}_3\text{Cr}_2\text{O}_8$ and $\text{Sr}_3\text{V}_2\text{O}_8$ could be indexed to the known¹¹ trigonal $R\bar{3}m$ (No. 166) structure and Rietveld refinements,¹² shown in Fig. 2, of the X-ray patterns gave the corresponding hexagonal lattice parameters $a = b = 5.5718(3)$ Å and $c = 20.1723(13)$ Å for $\text{Sr}_3\text{Cr}_2\text{O}_8$, and $a = b = 5.6215(4)$ Å and $c = 20.1152(15)$ Å for $\text{Sr}_3\text{V}_2\text{O}_8$. These values are in reasonable agreement with previously reported values for single crystalline $\text{Sr}_3\text{Cr}_2\text{O}_8$ ($a = b = 5.562$ Å, and $c = 20.221$ Å)¹¹ and polycrystalline $\text{Sr}_3\text{V}_2\text{O}_8$ ($a = b = 5.621$ Å, and $c = 20.14$ Å).¹³ Some parameters

TABLE I: Structure parameters for $\text{Sr}_3\text{Cr}_2\text{O}_8$ and $\text{Sr}_3\text{V}_2\text{O}_8$ refined from powder XRD data. The overall isotropic thermal parameter B is defined within the temperature factor of the intensity as $e^{-2B \sin^2 \theta / \lambda^2}$.

Sample	atom	x	y	z	B (\AA^2)	R_{wp}	R_p
$\text{Sr}_3\text{Cr}_2\text{O}_8$	Sr	0	0	0	0.029(2)	0.152	0.107
	Sr	0	0	0.2034(1)	0.019(1)		
	Cr	0	0	0.4047(2)	0.022(2)		
	O	0	0	0.3233(8)	0.047(4)		
	O	0.8331(7)	0.1669(7)	0.8980(3)	0.039(2)		
$\text{Sr}_3\text{V}_2\text{O}_8$	Sr	0	0	0	0.016(1)	0.194	0.147
	Sr	0	0	0.2026(1)	0.006(1)		
	V	0	0	0.4050(3)	0.009(2)		
	O	0	0	0.3340(7)	0.006(4)		
	O	0.8400(8)	0.1600(8)	0.8955(4)	0.028(3)		

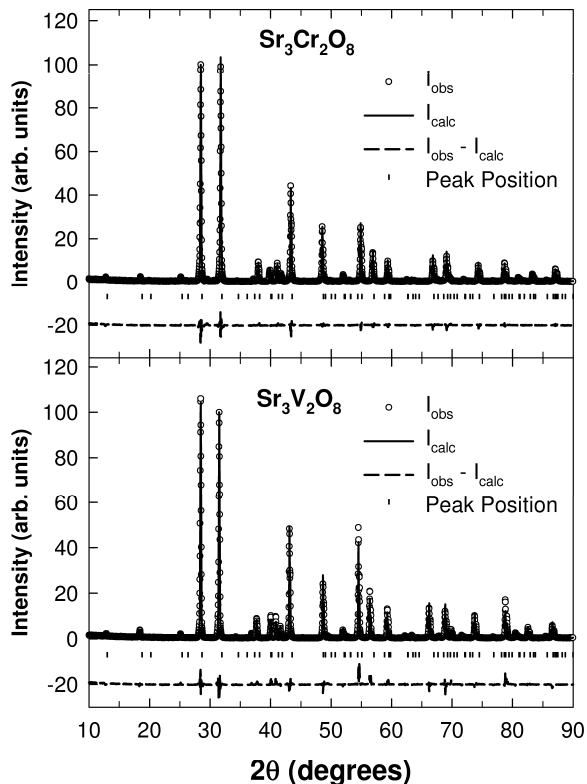


FIG. 2: Rietveld refinements of the $\text{Sr}_3\text{Cr}_2\text{O}_8$ and $\text{Sr}_3\text{V}_2\text{O}_8$ X-ray diffraction data. The open symbols represent the observed data, the solid lines represent the fitted pattern, the dotted lines represent the difference between the observed and calculated intensities and the vertical bars represent the peak positions.

obtained from the Rietveld refinements of our samples are given in Table I.

The observed magnetic susceptibility $\chi_{\text{obs}}(T)$ for $\text{Sr}_3\text{Cr}_2\text{O}_8$ is shown in Fig. 3. The $\chi_{\text{obs}}(T)$ follows a Curie-Weiss behavior between 100 K and 300 K. A fit to the

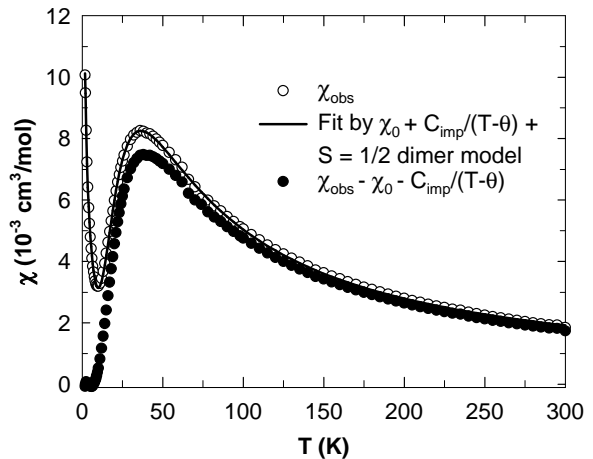


FIG. 3: The magnetic susceptibility χ versus temperature T for $\text{Sr}_3\text{Cr}_2\text{O}_8$. The open circles are the observed susceptibility χ_{obs} , the solid curve is a fit by an isolated dimer model Eq. (1) and the filled circles are the dimer spin susceptibility obtained by subtracting the constant term and the impurity term in Eq. (1) from χ_{obs} .

data (not shown in the figure) between 100 K and 300 K by the Curie-Weiss expression $\chi = \chi_0 + C/(T - \theta)$ gives $\chi_0 = -3.6(2) \times 10^{-4} \text{ cm}^3/\text{mol}$, $C = 0.76(1) \text{ cm}^3 \text{ K/mol}$ and $\theta = -40(2) \text{ K}$. The value of C corresponds to an effective moment of $1.74(1) \mu_B/\text{Cr}$ which is close to the value $1.72 \mu_B$ expected for Cr^{5+} ($S = 1/2$) moments with a g -factor of 1.98 taken from a previous EPR measurement.¹⁴ A negative θ indicates antiferromagnetic interactions between the Cr^{5+} moments. At lower temperatures χ exhibits a broad maximum at 38 K before decreasing sharply on cooling. The $\chi_{\text{obs}}(T)$ increases again below 6.5 K and this increase is most likely due to a small amount of paramagnetic impurities. The strong decrease towards zero in $\chi_{\text{obs}}(T)$ below 38 K suggests the presence of a spin-gap. The $\chi_{\text{obs}}(T)$ data in the complete

temperature range could be fitted by the expression

$$\begin{aligned}\chi_{\text{obs}} &= \chi_0 + \chi_{\text{imp}} + \chi_{\text{dimer}} \\ &= \chi_0 + C_{\text{imp}}/(T - \theta) + \frac{3C/T}{(3 + e^{\Delta/k_B T})},\end{aligned}\quad (1)$$

where χ_0 is a temperature independent term, χ_{imp} is the contribution from paramagnetic impurities with C_{imp} the Curie constant of the impurities and θ the Weiss temperature of the impurities, and χ_{dimer} is the contribution from isolated $S = 1/2$ dimers. The dimers have a spin-gap $\Delta = J_0$ from the singlet ground state to the spin-1 triplet excited states, and a paramagnetic Curie constant C . The fit gave the values $\chi_0 = 7(1) \times 10^{-5} \text{ cm}^3/\text{mol}$, $C_{\text{imp}} = 0.0297(3) \text{ cm}^3 \text{ K}/\text{mol}$, $\theta = -1.13(3) \text{ K}$, $C = 0.763(4) \text{ cm}^3 \text{ K}/\text{mol}$ and $\Delta/k_B = 61.9(1) \text{ K}$. The value of C is the same as that found from the above Curie-Weiss fit to the high temperature data. A very good fit is obtained over the whole temperature range as shown by the solid curve through the χ_{obs} data in Fig. 3. Also shown in Fig. 3 are the data after subtracting χ_0 and χ_{imp} from χ_{obs} , illustrating the spin susceptibility of the dimers.

To get an estimate of the interdimer interaction strengths J_1 , J_2 and J_3 in $\text{Sr}_3\text{Cr}_2\text{O}_8$ we can write the susceptibility by including these interactions as effective fields. The contribution to the susceptibility from interacting dimers can then be written as¹⁵

$$\chi_{\text{interactingDimer}} = \frac{\chi_{\text{Dimer}}}{1 + \gamma\chi_{\text{Dimer}}} = \frac{3C/T}{(3 + e^{\Delta/k_B T} + J'/T)},\quad (2)$$

where $\gamma = J'/3C$ is the molecular field constant, with $J' = 3J_1 + 6J_2 + 6J_3$, where J' is the sum of the interdimer exchange interactions. Fitting χ_{obs} by the expression

$$\chi_{\text{obs}} = \chi_0 + \chi_{\text{imp}} + \chi_{\text{interactingDimer}}\quad (3)$$

gives the value $J_0/k_B = 62.0(1) \text{ K}$ for the intradimer exchange interaction, which is very similar to the above value $61.9(1) \text{ K}$ obtained by fitting the data by Eq. (1), and $J'/k_B = 6(2) \text{ K}$ for the sum of the interdimer exchange interactions. The rms deviation of the fit from the data is $4.63 \times 10^{-5} \text{ cm}^3/\text{mol}$ for the isolated dimer model and the slightly smaller value of $4.55 \times 10^{-5} \text{ cm}^3/\text{mol}$ for the interacting dimer model. Thus there is little improvement in the fit by including an interaction between dimers.

The values of J_0 and J' indicate that the coupling between the dimers is weak or negligible compared to the coupling within a dimer. This is in contrast to the case of $\text{Ba}_3\text{Mn}_2\text{O}_8$ where $J_0/k_B = 17.4 \text{ K}$ is comparable to $J'/k_B = 8.3 \text{ K}$ [7] and the case of $\text{Ba}_3\text{Cr}_2\text{O}_8$ where $J_0/k_B = 25 \text{ K}$ is also comparable to $J'/k_B = 7.7 \text{ K}$.⁹ The nearest Cr-Cr distance in $\text{Sr}_3\text{Cr}_2\text{O}_8$ is 3.842 \AA whereas the corresponding distance between nearest Cr-Cr in $\text{Ba}_3\text{Cr}_2\text{O}_8$ is 3.934 \AA and between nearest Mn-Mn in $\text{Ba}_3\text{Mn}_2\text{O}_8$ is 3.984 \AA . The J_0 values for the Cr compounds indicate that the intradimer exchange interaction

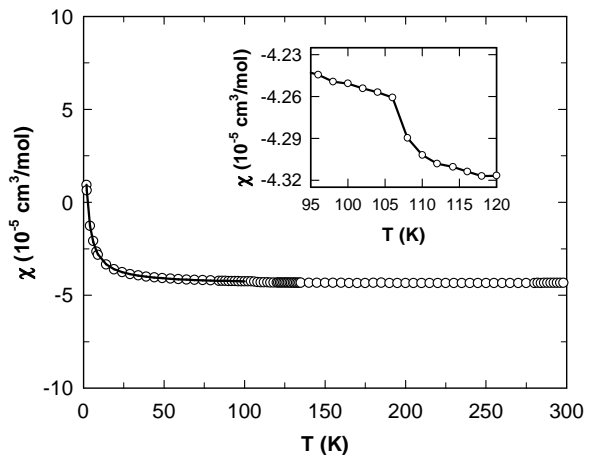


FIG. 4: The magnetic susceptibility χ versus temperature T for $\text{Sr}_3\text{V}_2\text{O}_8$. The solid curve through the data between 1.8 K and 100 K is a fit by the Curie-Weiss law. The inset shows the data between 95 K and 120 K on an expanded scale to show the transition at 110 K. The solid curve through the data in the inset is a guide to the eye.

decreases with increasing Cr-Cr distance, as qualitatively expected.

The magnetic susceptibility χ versus temperature T for $\text{Sr}_3\text{V}_2\text{O}_8$ is shown in Fig. 4 for $1.8 \text{ K} \leq T \leq 300 \text{ K}$. The $\chi(T)$ is almost temperature independent in the whole temperature range. The inset shows the χ data between 95 K and 120 K on an expanded scale to highlight a sharp step-like upturn in χ below 110 K. This is the onset of a bulk phase transition in $\text{Sr}_3\text{V}_2\text{O}_8$ as seen in the heat capacity measurement discussed next. Since there are no magnetic ions in the insulating $\text{Sr}_3\text{V}_2\text{O}_8$ compound, this phase transition is most likely a structural transition. The small upturn in the main panel at low temperatures could be fitted (solid curve) by a Curie-Weiss expression $\chi = \chi_0 + C/(T - \theta)$ with the values $\chi_0 = -4.5(1) \times 10^{-5} \text{ cm}^3/\text{mol}$, $C = 1.68(1) \times 10^{-4} \text{ cm}^3/\text{mol}$ (corresponding to about 0.2 mol% spin-1/2 impurities) and $\theta = -1.33(2) \text{ K}$.

The heat capacity C versus temperature T of $\text{Sr}_3\text{Cr}_2\text{O}_8$ and $\text{Sr}_3\text{V}_2\text{O}_8$ between 1.8 K and 300 K is shown in Fig. 5. There is no signature of any long-range magnetic ordering for $\text{Sr}_3\text{Cr}_2\text{O}_8$ which rules out the possibility of a magnetic transition at 38 K where the maximum in $\chi(T)$ was observed. The inset in Fig. 5 shows ΔC , obtained by subtracting the heat capacity of $\text{Sr}_3\text{V}_2\text{O}_8$ from that of $\text{Sr}_3\text{Cr}_2\text{O}_8$. The ΔC shows a maximum at about 22 K before decreasing rapidly towards zero at lower temperatures. The ΔC becomes negative above 50 K which indicates that the heat capacity for $\text{Sr}_3\text{V}_2\text{O}_8$ does not quantitatively represent the lattice heat capacity for $\text{Sr}_3\text{Cr}_2\text{O}_8$. The reason for this can be seen from Fig. 5 where a large heat capacity anomaly is seen at about 110 K in the data for $\text{Sr}_3\text{V}_2\text{O}_8$. The heat capacity peak occurs at the same temperature at which a step like anomaly was seen in the χ data for this sample and as stated above most

likely arises from a lattice transformation. This phase transition in $\text{Sr}_3\text{V}_2\text{O}_8$ at 110 K causes the heat capacity of $\text{Sr}_3\text{V}_2\text{O}_8$ to cross the data for $\text{Sr}_3\text{Cr}_2\text{O}_8$ at lower temperatures and leads to the negative ΔC values above 50 K. Although the ΔC may not be a quantitatively correct measure of the magnetic heat capacity of $\text{Sr}_3\text{Cr}_2\text{O}_8$, the qualitative shape of ΔC with a peak at about 20 K and a sharp decrease towards zero at low temperatures is what one would expect for the magnetic heat capacity of a spin dimer compound and confirms the presence of a spin gap in this material. The $C(T)$ data of $\text{Sr}_3\text{V}_2\text{O}_8$ between 1.8 K and 4 K could be fitted by the expression $C = \beta T^3$ and gave the value $\beta = 0.399(2)$ mJ/mol K⁴. From the value of β one can obtain the Debye temperature Θ_D using the expression¹⁶

$$\Theta_D = \left(\frac{12\pi^4 R n}{5\beta} \right)^{1/3}, \quad (4)$$

where R is the molar gas constant and n is the number of atoms per formula unit ($n = 13$ for $\text{Sr}_3\text{V}_2\text{O}_8$). We obtain $\Theta_D = 398(2)$ K for $\text{Sr}_3\text{V}_2\text{O}_8$. The low temperature $C(T)$ of $\text{Sr}_3\text{Cr}_2\text{O}_8$ has contributions from the paramagnetic impurities which led to an upturn in $\chi(T)$ at low temperatures, and could not be used to obtain Θ_D for this compound. The upturn in $C(T)$ at low temperatures is most likely due to a splitting of the magnetic ground state of the paramagnetic impurities by the crystalline electric field (CEF). The CEF splitting would give rise to a Schottky like anomaly in $C(T)$ and the upturn we observe is probably the high temperature tail of such an anomaly. This maximum of such a Schottky anomaly is expected to shift to higher temperatures on the application of a magnetic field. We have performed heat capacity measurements at different magnetic fields (not shown here) and we indeed see a broad Schottky-like anomaly peaked at around 5 K in the $C(T)$ data for a field of 1 T. This broad peak shifts upwards in temperature for fields of 5 T and 9 T and merges with the low temperature part of the dimer anomaly. We were unable to fit the data in all fields to a Schottky model with the same parameters. This indicates that there might be more than one species

of paramagnetic impurities which behave differently.

In conclusion, we have synthesized polycrystalline samples of the compounds $\text{Sr}_3\text{Cr}_2\text{O}_8$ and $\text{Sr}_3\text{V}_2\text{O}_8$ and studied their structural, magnetic and thermal properties. $\text{Sr}_3\text{Cr}_2\text{O}_8$ is a compound with chromium in the rare valence state Cr^{5+} ($S = 1/2$). The magnetic properties of $\text{Sr}_3\text{Cr}_2\text{O}_8$ are consistent with it being a new $S = 1/2$ spin-dimer compound where the nearest neighbour Cr^{5+} - Cr^{5+} ions couple antiferromagnetically to form spin-1/2 dimers with a singlet ground state separated from the excited triplet state by an energy gap $\Delta/k_B = 62$ K and a relatively weak interdimer coupling of about 6 K. The data for $\text{Sr}_3\text{V}_2\text{O}_8$ show that this compound undergoes a phase transition at about 110 K which is most likely a structural transition. The Debye temperature for $\text{Sr}_3\text{V}_2\text{O}_8$ is de

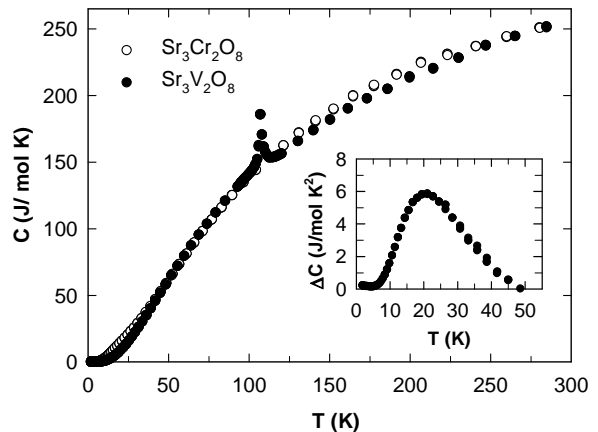


FIG. 5: The heat capacity C versus temperature T for $\text{Sr}_3\text{Cr}_2\text{O}_8$ and $\text{Sr}_3\text{V}_2\text{O}_8$. The inset shows the difference ΔC between the heat capacities of $\text{Sr}_3\text{Cr}_2\text{O}_8$ and $\text{Sr}_3\text{V}_2\text{O}_8$.

Acknowledgments

Work at the Ames Laboratory was supported by the Department of Energy-Basic Energy Sciences under Contract No. DE-AC02-07CH11358.

¹ T. Nikuni, M. Oshikawa, A. Oosawa, and H. Tanaka, Phys. Rev. Lett. **84**, 5868 (2000).
² T. Waki, Y. Morimoto, C. Michioka, M. Kato, H. Kageyama, K. Yoshimura, S. Nakatsuji, O. Sakai, Y. Maeno, H. Mitamura and T. Goto, J. Phys. Soc. Jpn. **73**, 3435 (2004).
³ M. Jaime, V. F. Correa, N. Harrison, C. D. Batista, N. Kawashima, Y. Kazuma, G. A. Jorge, R. Stern, I. Heinmaa, S. A. Zvyagin, Y. Sasago, and K. Uchinokura, Phys. Rev. Lett. **93**, 087203 (2004).
⁴ T. Radu, H. Wilhelm, V. Yushankhai, D. Kovrizhin, R. Coldea, Z. Tylczynski, T. Luhmann, and F. Steglich, Phys. Rev. Lett. **95**, 127202 (2005).

⁵ H. Kageyama, K. Yoshimura, R. Stern, N. V. Mushnikov, K. Onizuka, M. Kato, K. Kosuge, C. P. Slichter, T. Goto, and Y. Ueda, Phys. Rev. Lett. **82**, 3168 (1999); K. Kodama, M. Takigawa, M. Horvati, C. Berthier, H. Kageyama, Y. Ueda, S. Miyahara, F. Becca, and F. Mila, Science **298**, 395 (2002).
⁶ M. Uchida, H. Tanaka, M. Bartashevich and T. Goto, J. Phys. Soc. Jpn. **70**, 1790 (2001).
⁷ M. Uchida, H. Tanaka, H. Mitamura, F. Ishikawa, and T. Goto, Phys. Rev. B **66**, 54429 (2002).
⁸ H. Tsujii, B. Andraka, M. Uchida, H. Tanaka, and Y. Takano, Phys. Rev. B **72**, 214434 (2005).
⁹ T. Nakajima, H. Mitamura, and Y. Ueda, J. Phys. Soc.

- Jpn. **75**, 054706 (2006).
- ¹⁰ T. Negas and R. S. Roth, J. Res. Natl. Bur. Stds. A **73**, 431-442 (1969).
- ¹¹ E. Cuno and H. Mueller-Buschbaum, Z. anorg. allg. Chem. **572**, 95 (1989).
- ¹² Rietveld analysis program DBWS-9807a release 27.02.99, ©1998 by R. A. Young, an upgrade of "DBWS-9411 - an upgrade of the DBWS programs for Rietveld Refinement with PC and mainframe computers, R.A. Young, J. Appl. Cryst. **28**, 366 (1995)".
- ¹³ A. Durif, Acta Cryst. **12**, 420 (1959).
- ¹⁴ M. Gaft, G. Boulon, G. Panczer, Y. Guyot, R. Reifeld, S. Votyakov, and G. Bulka, J. Lumin. **87-89**, 1118 (2000).
- ¹⁵ D. C. Johnston, in *Handbook of Magnetic Materials*, Vol. 10, Pg.1, edited by K. H. J. Buschow (Elsevier Science B. V., Netherlands, 1997).
- ¹⁶ C. Kittel, *Solid State Physics* (John Wiley and Sons, Inc., New York, 1966).